05,11

# Magnetic anisotropy in TbFeB and PrDyFeCoB microwires

© V.L. Sidorov[1], O.V. Kopkak[1], D.V. Korolev[2], V.P. Piskorskii[2], R.A. Vallev[2], R.B. Morgunov[1,2,3]

[1] Federal Research Center for Problems of Chemical Physics and Medical Chemistry of the Russian Academy of Sciences, Chernogolovka, Russia
[2] All-Russian Scientific Research Institute of Aviation Materials National Research Center „Kurchatov Institute", Moscow, Russia
[3] Federal State Autonomous Educational Institution for Higher Education „Immanuel Kant Baltic Federal University", Tambov, Russia

E-mail: morgunov2005@yandex.ru

*Received October 27, 2022*
*Revised October 27, 2022*
*Accepted November 2, 2022*

$Tb_7Fe_90B_3$ microwires with a diameter of $50-100\,\mu$m were obtained by the method of ultrafast cooling of the melt. It has been established that the microwires contain the tetragonal $Tb_2Fe_{14}B_1$ phase and the cubic $TbFe_3$ phase. These two phases differ in saturation fields of 100 Oe and 10 kOe, respectively. The anisotropy of the coercive force of TbFeB microwires also indicates the coexistence of two magnetic phases. The data obtained are compared with the magnetic properties of PrDyFeCoB microwires, in which the coercive force is isotropic, and magnetization saturation is achieved in lower fields.

**Keywords:** magnetic anisotropy, shape anisotropy, single-ion anisotropy, tetragonal phase, microwires.

DOI: 10.21883/PSS.2023.02.55408.518

## 1. Introduction

RE-TM-B microwires by obtained ultrafast melt cooling are the items whose magnetic properties are considerably different from bulk materials [1–3]. Multiple differences are due to the fact that the phase formation process and a set of stable (but not always equilibrium) phases in microwires differ considerably from a set of typical phases in bulk rare-earth magnets. High cooling rate holds non-equilibrium phases in the melt, and high internal voltages stabilized in microwires at a high cooling rate influence magnetization because this type of alloys feature abnormally high magnetoelastic constants [4]. In addition, limited microwire dimensions in two directions result in the appearance of the main magnetic axis along the microwire axis and facilitates microcrystalline state texturization by limiting potential grain growth directions.

The main magnetic phase of $Tb_2Fe_{14}B$ has tetragonal symmetry with crystalline lattice parameters $a = 58.764$ Å, $c = 12.031$ Å, $c/a = 1.373$ at room temperature and Curie temperature $T_c = 646$ K [5]. Saturation magnetization of such phase per lattice cell is $14\,\mu_B$, which corresponds to antiparallel orientation of magnetic moments of magnetic moments of $Tb^{3+}$ sublattice $4f^8$ (orbital momentum $L = 3$, spin momentum $S = 3$, total momentum $J = 6$) and iron ion sublattice. Axial single-ion anisotropy field of $Tb^{3+}$ is 140 kOe at 300 K, which is the highest anisotropy field among rare-earth ions.

Single-ion anisotropy of rare-earth ions in the aforesaid alloys occurs as a result of ion energy level splitting by a crystalline field that orients the orbital momentum of Tb, Dy, Pr magnetic ion etc. with ellipsoid shape of $4f$-electron shell [6,7]. Terphenol $TbFe_2$ is known to have one of the strongest positive magnetostrictions at room temperature [8,9], however, due to high single-ion anisotropy of cubic Laves phases of terbium, this is manifested only in rather high magnetic fields [8] for magnetic saturation and maximum magnetostriction achievement.

Cubic Laves phase $ReFe_2$, where $Re$ — are rare earth elements, generally shows huge magnetostriction at room temperature due to strong spin-orbital interaction between the electron spin and spatially-anisotropic $4f$-electron cloud [10]. This phase in macroscopic specimens generally has high magnetocrystalline anisotropy leading to rather high magnetic fields required for magnetization saturation and magnetostriction [10]. Saturation magnetostriction of $TbFe_3$, $TbFe_2$ phases known as intermetallide variations is referred in literature as one of the highest among all materials [10].

Temperature dependences of magnetization in amorphous alloys $Tb_x(Fe_{82}B_{18})_{100-x}$, $x = 0-50$ at.% were obtained in [11]. It has been found that spin glass freezing temperature varied in the range from 70 to 140 K and Curie temperature of such alloy varied from 291 to 600 K, depending on the terbium concentration. In microwires composed of $Tb_x(Fe_{82}B_{18})_{100-x}$ obtained by hanging melt drop extraction, higher terbium content ($x = 30$)

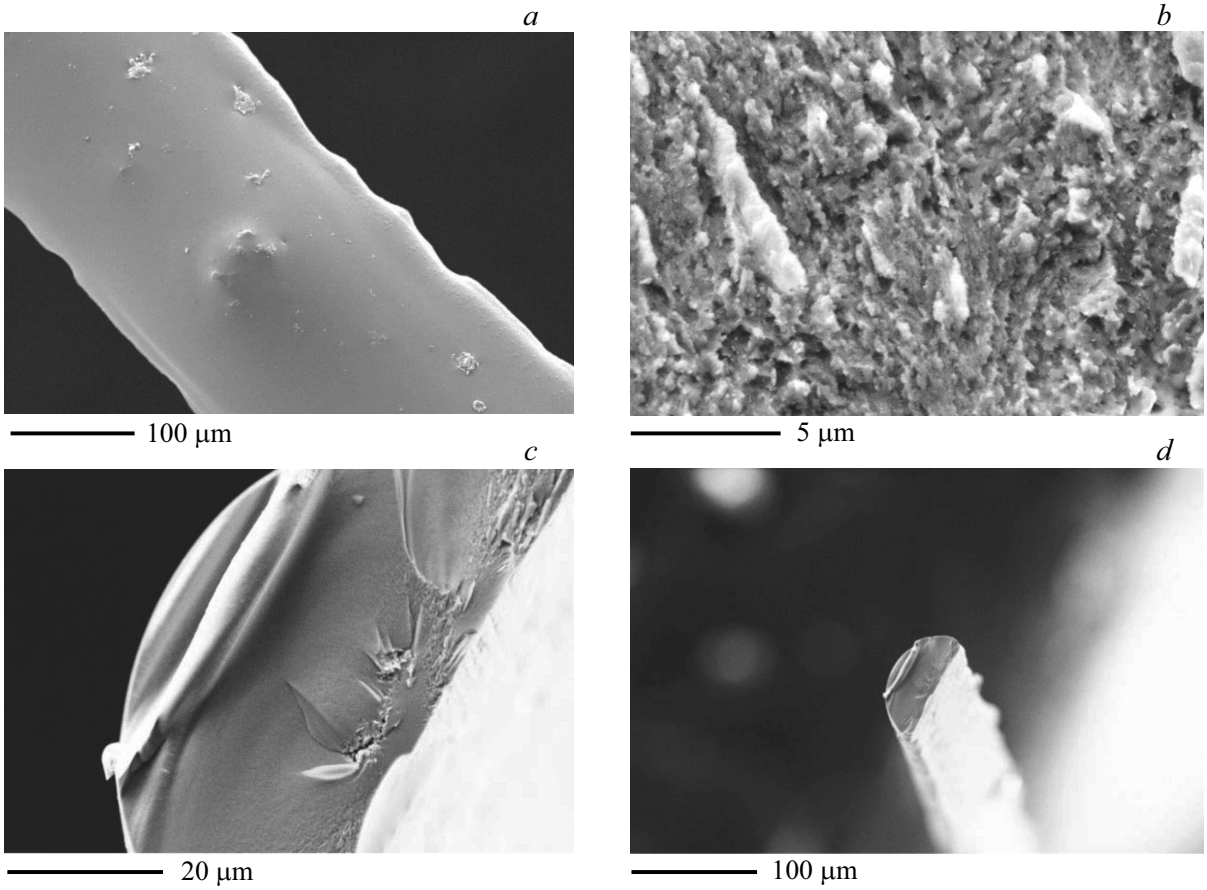


**Figure 1.** SEM images of TbFeB microwire.

ensured high magnetostriction and prevailing single-axis anisotropy [11]. At low terbium content ($x = 10$ at.%), magnetostriction stresses were low and cubic symmetry prevailed.

In [12], TbFeB nanoparticles 8 to 80 nm in size were examined. It has been found that coercive force in large particles 50−80 nm in size achieved 22.1 kOe, while reduced particle sizes up to 8 nm resulted in lower coercive force up to 400 Oe. It has been demonstrated that the coercive force difference was caused by transition from multiple domain system in large particles to small single domain particles.

The purpose of this study was to produce TbFeB microwires, determine phase and chemical composition, to study their magnetic anisotropy and to compare it with the anisotropy in previously produced PrDyFeCoB microwires with similar type of rare-earth ions $Dy^{3+}$ and $Pr^{3+}$.

## 2. Experimental procedure and specimens

TbFeB microwires were obtained by a hanging melt drop extraction method. The melt was produced by heating sintered $Tb_7Fe_{90}B_3$ magnet face by an electron beam. A melt drop was captured by a rapidly rotating water-cooled brass cylinder that stretched the drop into a long microwires. Cooling rate during thermal contact with the cylinder was about $\sim 10^5$ K/s. At high cylinder linear speeds $\sim 40-50$ m/s, microwires with a diameter of $50-100\,\mu$m and a length of 5−10 mm are produced (Figure 1, $a-d$). Microwires have a semi-cylinder shape. A microwire used for testing was 2 mm long with a semi-cylinder diameter of 88 $\mu$m.

Magnetic moment of microwires $m$ was measured using MPMS XL Quantum Design magnetometer in magnetic fields $H = 0-50$ kOe. External magnetic field was directed along and at right angle to the microwire axis. Field dependences of magnetization $M(H)$ were obtained with a slow isothermal magnetic field growth so that each of them was measured at a fixed cryostat temperature. Scanning electron microscope (SEM) images of microwires were obtained using the Tescan Clara ultra high resolution system at 15 kV accelerating voltage on a cross-section cut prepared by ion etching and polishing in Technoorg Linda SEMPrep2 system. X-ray diffraction analysis of microwires was carried out using DRON-UM2 automated X-ray diffractometer with a copper tube ($CuK_\alpha$ line).

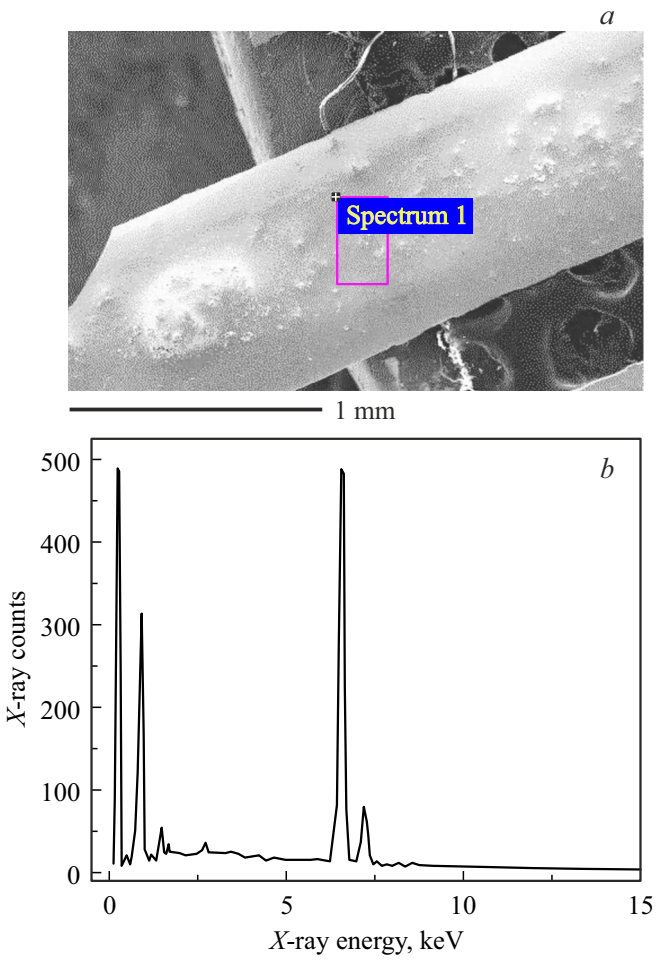


**Figure 2.** ($a$) SEM image fragment of the microwire with indicated EDX analysis area; ($b$) EDX spectrum of TbFeB microwire.

Structural and chemical analysis of PrDyFeCoB wires used herein for comparison is described in [13,14].

## 3. Experimental findings

### 3.1. Structure and chemical analysis of the microwires

TbFeB microwire fragment and it energy-dispersive analysis (EDX) spectrum are shown in Figure 2, $a$ and $b$, respectively. EDX spectrum analysis helped to carry out chemical analysis of the microwire near the specimen surface (Table). It is shown that Fe, Tb, B (concentration of the latter was determined by its atomic structure in the specimen before extraction, because this element cannot be determined by the EDX method) are the main elements in the microwire. The rest elements Pr, Dy, Fe, Cu, Ni were found in negligible quantities $< 0.1\%$.

Figure 3 shows energy-dispersive X-ray analysis (EDX) of TbFeB microwire in the form of Pr, Dy, Tb, Fe, Cu, Ni distributions determined in the designated microwire

Content of chemical elements in the microwire determined by EDX method

| Element | Atomic, % |
|---|---|
| Fe | 90.69 |
| Tb | 6.62 |
| Cu | 0.02 |
| Ni | 0.04 |
| Pr | 0.13 |
| Dy | 0.02 |
| B | 2.48 |
| Total | 100 |

area (Figure 3, $a$–$f$). Increased brightness corresponds to increased concentration of each element. The main elements Fe and Tb are rather evenly distributed over the scanned area. Those elements that were detected in trace quantities are distributed unevenly (except Dy). Ni, Cu and Pr are most probably at $\sim 50-100\,\mu$m grain boundaries according to the size of areas depleted in these elements (Figure 3, $b$–$d$).

For comparison, Figure 4 shows X-ray images for Tb-Fe-B microwires herein (Figure 4, $a$) and for $\sim 80$ nm Tb-Fe-B flakes studied in [12] (Figure 4, $b$), and $TbFe_3$ bulk specimens (Figure 4, $c$) [15]. In both cases, large number of peaks indicates that microwires and flakes are

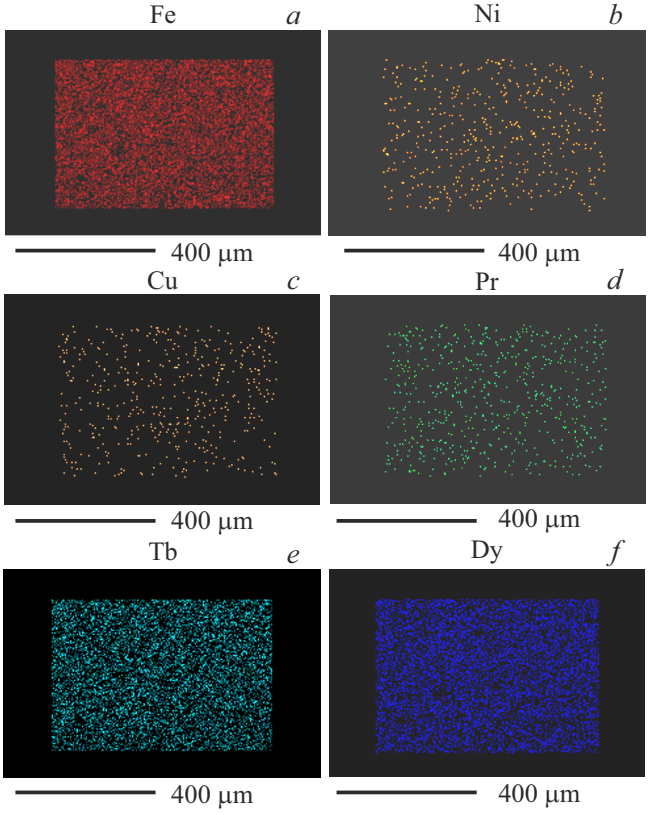


**Figure 3.** Chemical element distribution on TbFeB microwire fragment determined by the EDX method.

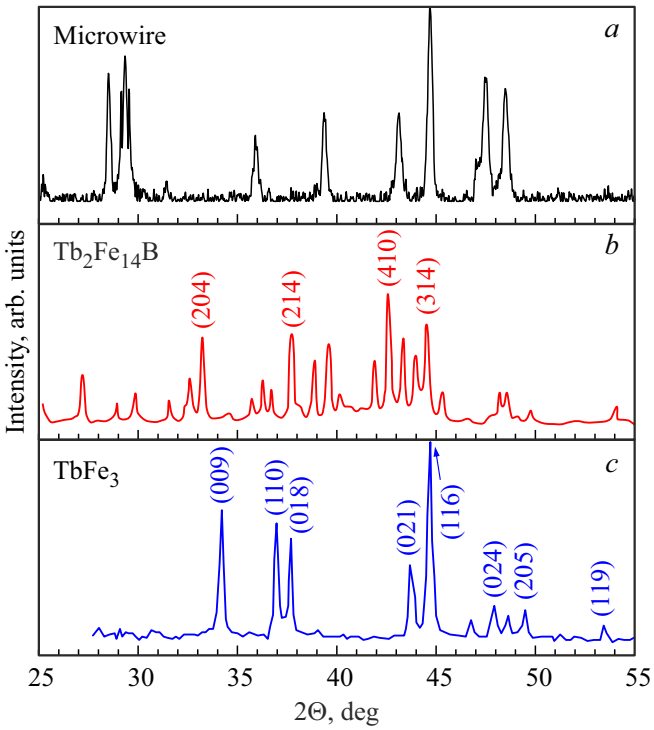


**Figure 4.** X-ray diffraction spectra of TbFeB microwires herein (black line) ($a$), for tetragonal phase $Tb_2Fe_{14}B$ according to [12] (red line) ($b$), for phase $TbFe_3$ (blue line) in [15] ($c$).

polycrystalline. In this case, no line widening typical of nanostructured material is observed in microwires. Comparison of Figure 4, $a$ with Figure 4, $b$ corresponding to tetragonal phase 2-14-1 shows that tetragonal crystalline structure $Tb_2Fe_{14}B$ is present in the microwires of interest, though, peaks are slightly shifted relative to the corresponding peaks in [12]. In addition to tetragonal phase, the specimens contain $TbFe_3$ phase (Figure 4, $c$) [15] that gives peaks at $2\theta > 45°$ corresponding to $R3m$ symmetry structure with crystalline lattice parameters $c = 2.463$ nm and $a = 0.514$ nm. No any obvious amorphous component content was recorded because no widened background is present on the diffraction pattern.

### 3.2. Magnetic properties of microwires

Magnetic moment dependences of TbFeB microwire on field $m(H)$ are shown in Figure 5, $a$ for a setof angles $\alpha$ between the field and microwire at $T = 300$ K. It is shown that a low-field portion quickly achieves the level which is the same for all angles and then quasi-linear growth of $m$ is observed with the field growth, while the slope of this dependence section $m(H)$ in strong fields depends considerably on angle $\alpha$. Such field dependence view generally implies that phase 1 with weak saturation field and phase 2 with strong saturation field are present. Figure 5, $b$ shows a fragment of $m(H)$ dependences in weak fields. It is shown that microwave rotation causes minor variations of coercive force $H_c$. Angular dependence $H_c(\alpha)$ is shown in Figure 5, $c$. This implies that coercive force variations with angle change are close to an error which occurs during specimen rotation. Thus, coercive force rather characterizes isotropic phase 1, while anisotropic phase 2 shows no obvious coercive force.

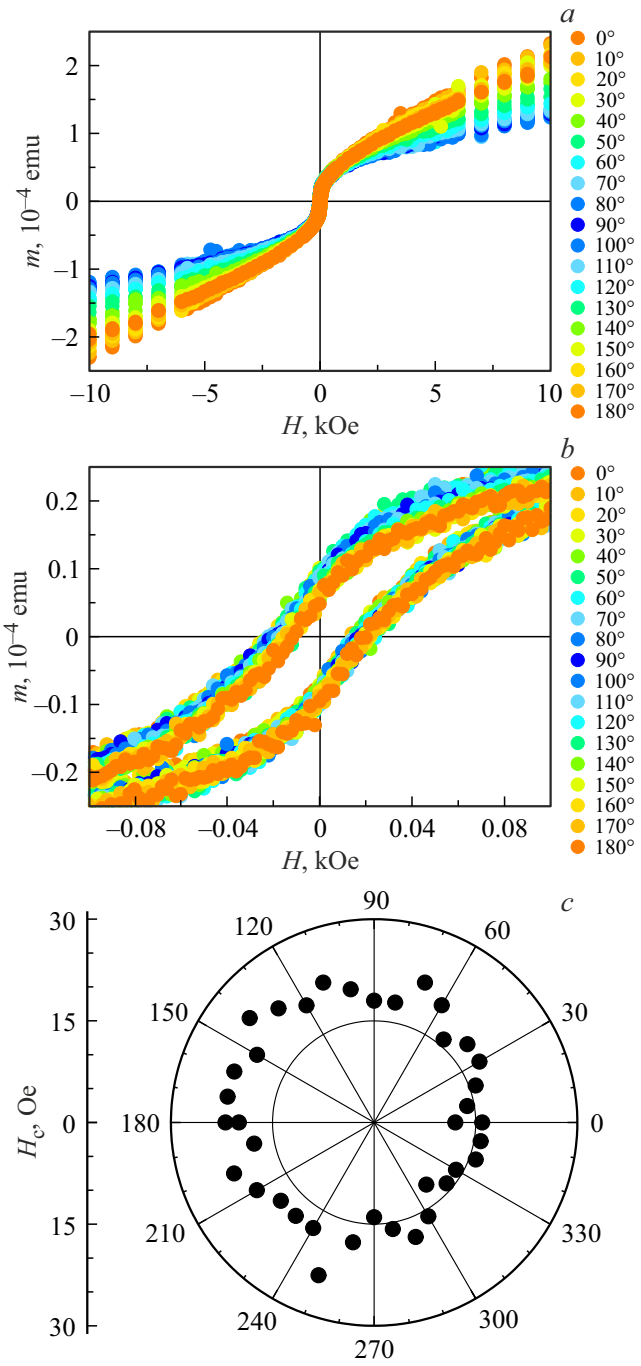


**Figure 5.** Dependences of magnetic moment $m$ of TbFeB microwire at 300 K on magnetic field $H$ shown in various field ranges 10 kOe ($a$), and 0.1 kOe ($b$); dependence of microwire coercive force $H_c$ on angle $\alpha$ between the magnetic field and microwire ($c$).

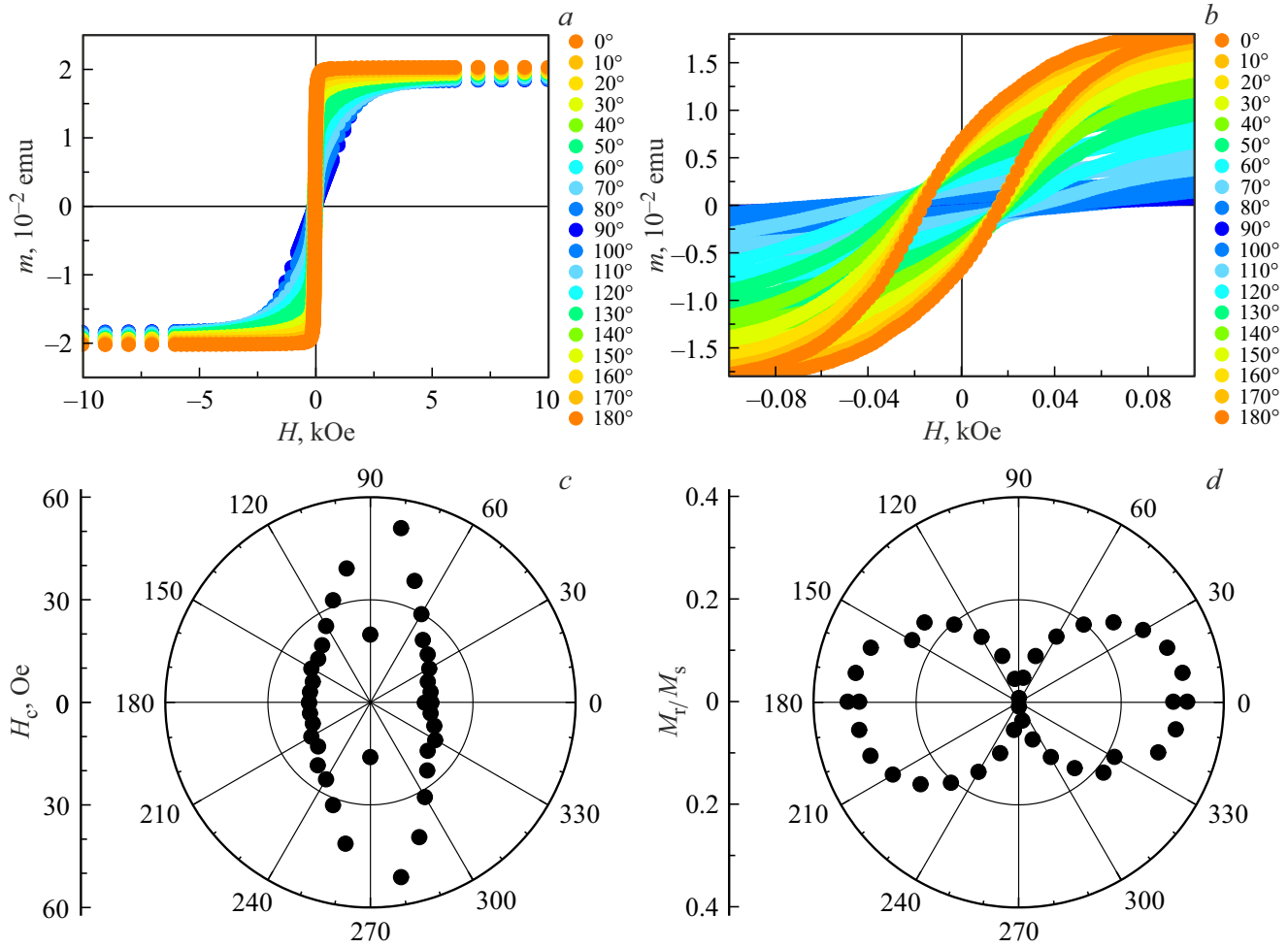


**Figure 6.** Dependences of magnetic moment $m$ of DyPrFeCoB microwire at 300 K on magnetic field $H$ shown in different field ranges 10 kOe ($a$), and 0.1 kOe ($b$); dependence of microwire coercive force $H_c$ on the angle between the magnetic field and microwire axis ($c$); dependence of the residual magnetization vs. saturation magnetization $M_r/M_s$ on angle $\alpha$ between the magnetic field and microwire axis ($d$).

Thus, the obtained data on angular dependence of TbFeB microwire magnetization hysteresis suggests that the microwire has two magnetic phases which differ in that magnetization saturation in phase 1 is achieved at 300−400 Oe, and there is magnetic hysteresis with coercive force $H_c$. Magnetization at which hysteresis loop collapses and phase 1 coercive force does not depend on angle $\alpha$ between the field and microwire axis. Phase 2 is most likely characterized by much lower coercive force, however, it shows very high saturation field and, respectively, strong magnetic anisotropy field $H_A$. This phase shows strong saturation field anisotropy which is not achieved in the accessible field variation interval up to 1−2 T at 300 K.

For comparison, field dependences and magnetic moment hystereses $m(H)$ were obtained in PrDyFeCoB microwires (Figure 6, $a$). In these microwires produced in the same conditions as TbFeB microwires, saturation was achieved even in weak fields $\sim$ 200 Oe. And magnetic moment hysteresis was observed in weak fields (Figure 6, $b$). In contrast to TbFeB microwires, coercive force in PrDyFeCoB specimens was considerably anisotropic and varied from the minimum value of 15 Oe in the field along the microwire axis to the maximum value of 60 Oe in the field at right angle to the microwire. A minor deviation from the true perpendicular direction at 10° was observed due to the competition between magnetocrystalline anisotropy and form anisotropy (Figure 6, $c$). Possible achievement of saturation magnetization allowed to plot the dependence of residual magnetization vs. saturation magnetization $M_r/M_s$ on angle $\alpha$ between the magnetic field and PrDyFeCoB microwire axis (Figure 6, $d$). This parameter was anisotropic. The obtained data demonstrates that the main magnetization axis extends along the microwire axis (direction with the lowest $H_c$ and highest $M_r/M_s$). It has been shown before that microwires have nanostructured phase 2-14-1 and amorphous phase [14].

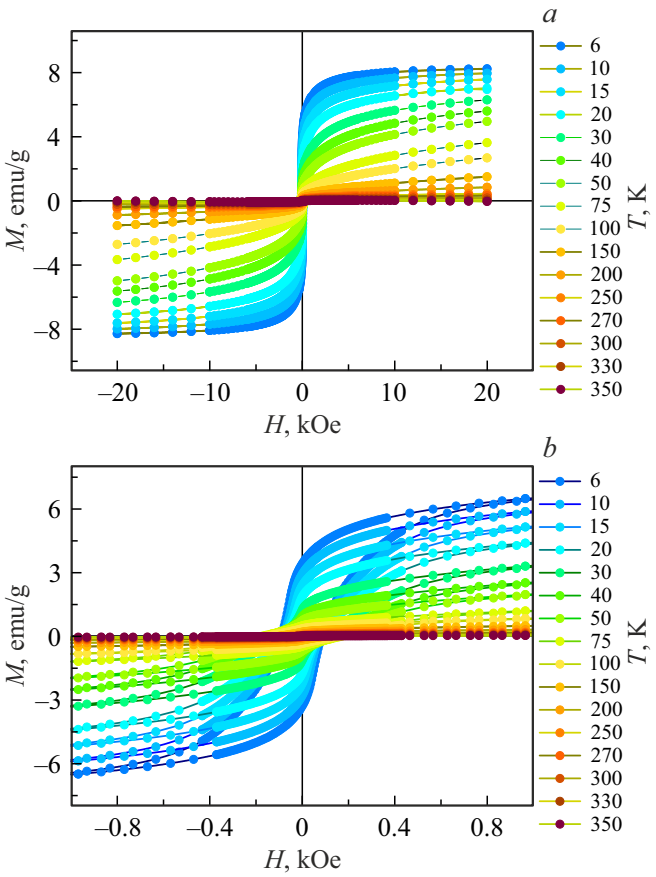


**Figure 7.** A set of hysteresis loops $M(H)$ of TbFeB microwire in the temperature range from 6 to 350 K. *a* — are loops $M(H)$ in full range (±20 kOe), *b* — is the same data in the weak field area (−150 Oe to +150 Oe). Magnetic field was applied along the microwire axis.

A set of magnetization hysteresis loops was obtained for TbFeB microwires at various temperatures from 6 to 350 K in the magnetic field along the microwire axis (Figure 7, *a, b*). Figure 8, *a* shows that coercive force $H_c$ varies in a nonmonotonous way when TbFeB temperature increases. There is a low-temperature drop-down section $H_c$ within 6−15 K. Then the coercive force grows up to 95 K and decreases again in the range from 100 to 350 K. The temperature growth causes monotonous reduction of residual magnetization $M_r$ and saturation magnetization $M_s$ (Figure 8, *b, c*, respectively). In this case, magnetization saturation at low temperatures is achieved in much lower fields that at high temperatures. At 6 K, saturation magnetization $M_s = 8.3$ emu/g occurs even at 5 kOe in TbFeB microwires.

## 4. Discussion

Field dependences of TbFeB microwire magnetization at 300 K are characterized by the absence of saturation $M_s$ even at higher magnetic fields (Figure 5). At the same time, sharp change in $m(H)$ slope is observed in field ∼ 100−200 Oe at which magnetic hysteresis loop „collapses". This suggests that there are two phases 1 and 2 whose magnetic contributions form the hysteresis loop. The first phase is characterized by low $M_s \sim 100-200$ Oe, and the second phase has $M_s$ higher than 10 kOe at 300 K. It can be seen that the magnetic moment in the second phase tends to saturation faster when the magnetic field is directed along the microwire axis than when the field and microwire are oriented at right angle. This means that the easy axis of phase 2 is directed along the microwire axis. In phase 1, achievement of saturation by the magnetic moment does not depend on the magnetic field orientation relative to the microwire. Using the maximum achievable magnetization of the microwire $M(1\,\text{T}) = m/\text{V} = 2.1 \cdot 10^{-4}\,\text{emu}/6 \cdot 10^{-6}\,\text{cm}^3 = 35\,\text{emu/cm}^3$ in field 1 T, the corresponding form anisotropy field can be calculated using the following approximation equation for cylinder $H_{\text{sh}} \sim 2\pi M(1\,\text{T}) = 219$ Oe. This form anisotropy field value cannot explain the observed magnetization anisotropy in high fields at 300−350 K.

Coercive force ∼ 200 Oe (Figure 5) is much lower than in previously studied alloys $Tb_2Fe_{14}B$. In [12], $H_c$ of alloy with dominant phase $Tb_2Fe_{14}B$ depended on the particle size and was maximum for 30 nm particles, and for particles larger than 100 nm, coercive force was reduced to 2−3 kOe. Therefore, there is reasonable cause to believe that the measured coercive force and field dependence of the microwire magnetic moment depend on the superposition of the appropriate coercive forces $H_{c1}$ and $H_{c2}$ and field dependences of these phases.

Magnetic property comparison between TbFeB specimens and PrDyFeCoB microwires shows that phase 1 in TbFeB with low-field saturation and hysteresis is similar to nanostructured phase 2-14-1 in PrDyFeCoB. This phase is also identified on the diffraction pattern (Figure 4). Low coercive forces mean that this phase is presented in the microwire in the form of nanoscale grains. Therefore, large grains whose sizes can be inferred by the chemical element distribution in Figure 3 are most likely $TbFe_3$ phase grains. This phase is well known to have very high saturation field which meets the obtained experimental data (Figure 5).

Magnetization hysteresis loop parameter variations of TbFeB microwires with temperature (Figure 8, *a*−*c*) can be explained by the competition of various types of magnetic anisotropy. Since the saturation magnetization of TbFeB microwires when cooled from 300 to 6 K increases from 0.056 emu/g to 8.3 emu/g, i.e. by a factor of ∼ 15 the form anisotropy field also increases in direct proportion. Taking into account the aforesaid assessment, it becomes equal to 3.3 kOe, which can be adequately comparable with volumetric anisotropy field $H_A$ of the alloy.

In order to assess the crystalline magnetic anisotropy field of TbFeB microwires, field dependence of magnetization

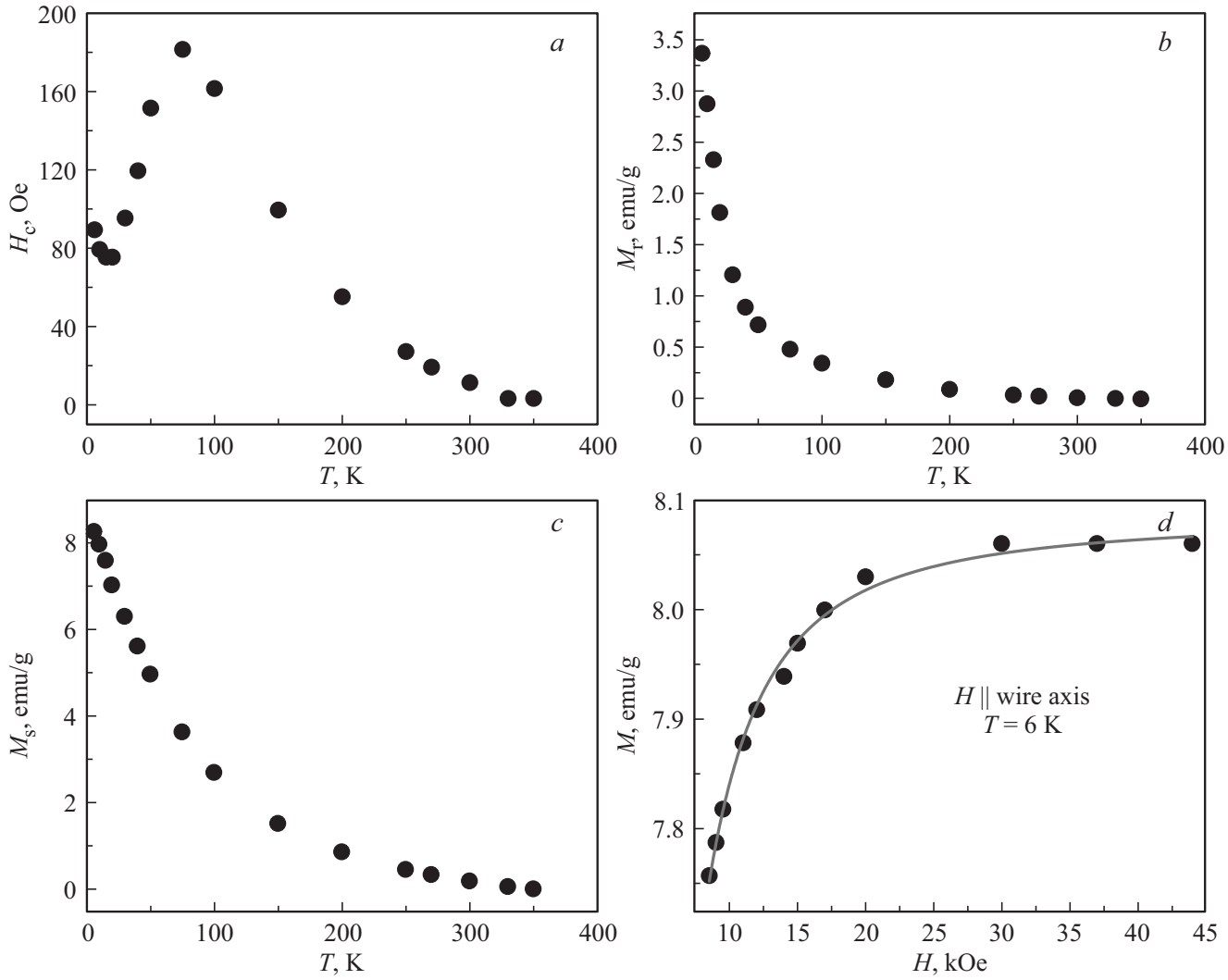


**Figure 8.** Temperature dependences of magnetization hysteresis loops of TbFeB specimen: coercive force $H_c$ ($a$), residual magnetization $M_r$ ($b$) saturation magnetization $M_s$ ($c$). High-field loop segment $M(H)$ of TbFeB microwire at 6 K approximated using Akulov equation [16,17] ($d$).

$M(H)$ was approximated at 6 K in the growing field using Akulov equation [16,17]:

$$M(H) = M_s(1 - 4K_1^2/15M_s^2H^2 - 64K_1K_2/105M_s^2H^2 - 128K_2^2/315M_s^2H^2) + \chi H, \quad (1)$$

The approximation using equation (1) is shown in Figure 8, $d$ with a solid line for temperature 6 K. First-order magnetic anisotropy constant $K_1 = 5.3 \cdot 10^5$ erg/cm$^3$ and second-order magnetic anisotropy constant $|K_2| = 3.8 \cdot 10^5$ erg/cm$^3$ are derived from it. The first-order anisotropy constant is in line with the literature data for intermetallide $K_1 = 6 \cdot 10^5$ erg/cm$^3$ [18,19]. With saturation magnetization $M_s = 8.0745$ emu/g, anisotropy field $H_A = 2K_1/M_s = 17.4$ kOe in TbFeB microwires at 6 K.

Another anisotropy field determination method includes comparison of dependences $M(H)$ recorded for two orthogonal field orientations relative to the microwire. Therefore, we have obtained high-field dependences $M(H)$ of TbFeB microwire with parallel and perpendicular field orientations $H$ at different temperatures (Figure 9, $a$, $b$). When the intersections of these dependences at different temperatures had been defined (see the example for 6 K in the Detail in Figure 9, $c$), temperature dependence for anisotropy field $H_A(T)$ was plotted (Field 9, $c$). At 6 K, the obtained anisotropy field $H_A = 18$ kOe conversion into the anisotropy constant gives $K_1 = 5.5 \cdot 10^5$ erg/cm$^3$, which meets the value calculated using Akulov equation for TbFeB microwire.

## 5. Conclusion

Ultrafast cooling of TbFeB melt was used to produce microwires where two magnetic phases were identified. $Tb_2Fe_{14}B$ phase has low saturation field $\sim 200$ Oe and

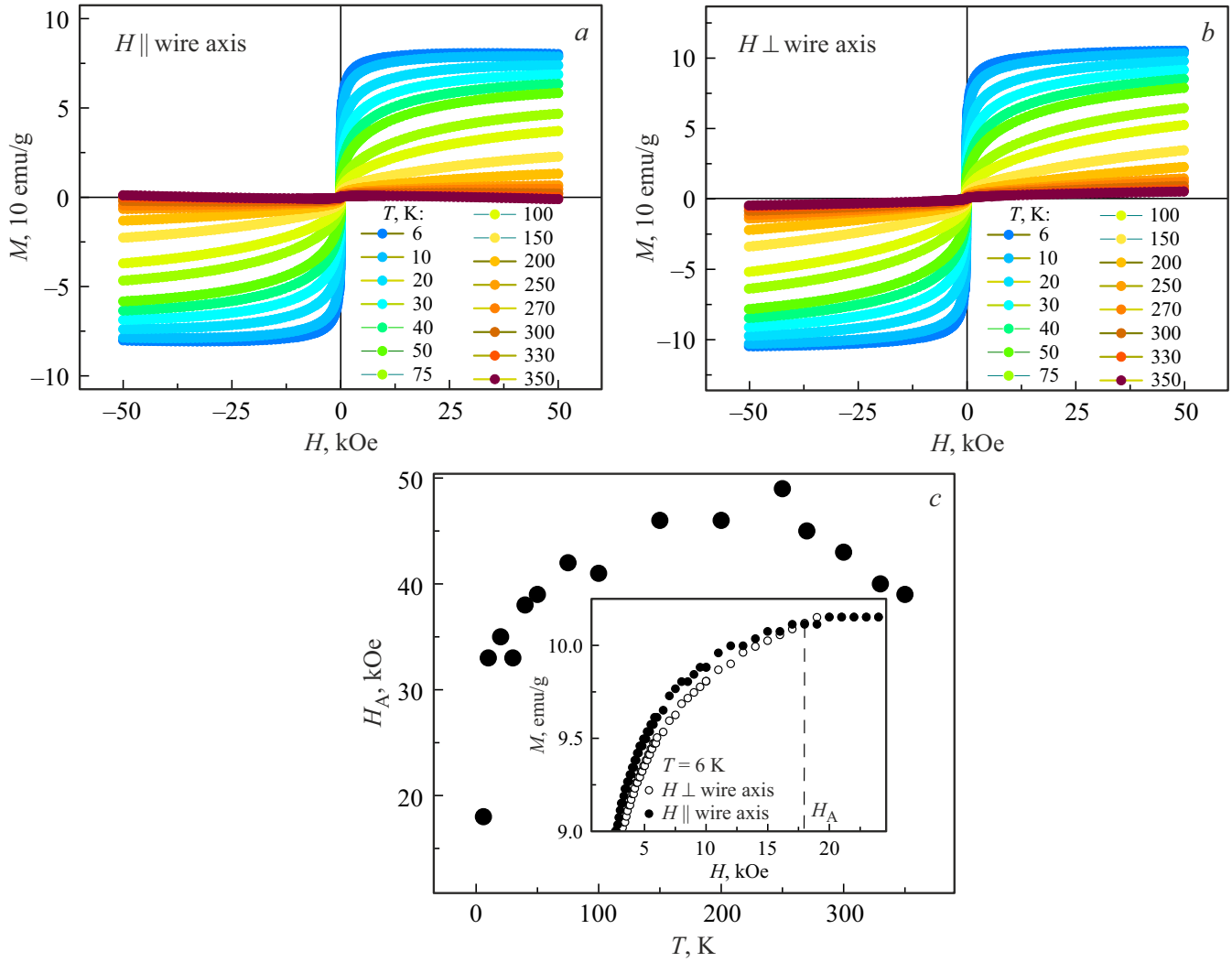


**Figure 9.** High-field dependences of TbFeB microwire magnetization with parallel orientation ($a$) and perpendicular orientation ($b$) of field $H$. Temperature dependence of anisotropy field $H_A$ for TbFeB microwire ($c$). The detail shows normalized magnetization curves with parallel and perpendicular orientation of external field relative to the long axis of the microwire at $T = 6$ K. $H_A$ was determined at the intersection of curves.

isotropic coercive force 15 Oe. Low coercive force of this phase means that the phase consists of nanoscale grains. Other $TbFe_3$ phase has a high saturation field which exceeds field 1 T obtained experimentally and zero coercive force. Grain sizes of this phase are from 200 to 300 $\mu$m. Strong single-phase anisotropy of terbium results in very high anisotropy field values in TbFeB microwires compared with that of PrDyFeCoB microwires.

## Funding

The study was carried out within theme map AAAA-A19-119092390079-8 of the Federal Research Center for Problems of Chemical Physics and Medical Chemistry (RSF grant No. 22-19-20157 and subsidy from the budget of the Kaliningrad Region No. 06-C/2022, https://rscf.ru/project/22-19-20157/, No. 22-19-20157).

## Conflict of interest

The authors declare that they have no conflict of interest.

## References

[1] S.Y. Kang, S.R. Lee, S.H. Lim. IEEE Trans. Magn. **35**, *5*, 3826 (1999). https://doi.org/10.1109/20.800678
[2] Z. Ren, L. Chen, S. Li, H. Liu, Z. Lu. IOP Conf. Ser.: Mater. Sci. Eng. **103**, 012006 (2015). https://doi.org/10.1088/1757-899X/103/1/012006
[3] S. Zhang, M. Zhang, Y. Qiao, X. Gao, D. Ling, S. Zhou. J. Magn. Magn. Mater. **322**, *16*, 2304 (2010). https://doi.org/10.1016/j.jmmm.2010.02.031
[4] H. Chiriac, T.-A. Óvári, A. Zhukov. J. Magn. Magn. Mater. **254–255**, 469 (2003). https://doi.org/10.1016/S0304-8853(02)00875-2

[5] A.T. Pedziwiatr, H.Y. Chen, W.E. Wallace. J. Magn. Magn. Mater. **67**, *3*, 311 (1987). https://doi.org/10.1016/0304-8853(87)90189-2
[6] J. Bland. A Mössbauer Spectroscopy and Magnetometry Study of Magnetic Multilayers and Oxides. University of Liverpool (2002).
[7] J.D. Rinehart. Long. Chem. Sci. **2**, *11*, 2078 (2011). https://doi.org/10.1039/C1SC00513H
[8] T. Shima, H. Yokoyama, H. Fujimori. J. Alloys Compd **258**, *1–2*, 149 (1997). https://doi.org/10.1016/S0925-8388(97)00058-3
[9] G.J. Bowden, P.A.J. de Groot, J.D. O'Neil, B.D. Rainford, A.A. Zhukov. J. Phys.: Condens. Matter **16**, *13*, 2437 (2004). https://doi.org/10.1088/0953-8984/16/13/021
[10] J.-C. Shih, S.-Y. Hsu, L.-J. Chao, T.-S. Chin. J. Appl. Phys. **88**, *6*, 3541 (2000). https://doi.org/10.1063/1.1286469
[11] S.J. Clegg, R.D. Greenough, W.E. Hagston. J. Appl. Phys. **73**, *10*, 5589 (1993). https://doi.org/10.1063/1.353660
[12] R.M. Liu, M. Yue, W.Q. Liu, D.T. Zhang, J.X. Zhang, Z.H. Guo, W. Li. Appl. Phys. Lett. **99**, *16*, 162510 (2011). https://doi.org/10.1063/1.3653256
[13] D.V. Korolev, R.A. Valeev, V.P. Piskorsky, O.V. Koplak, O.S. Dmitriev, A.D. Talantsev, R.B. Morgunov. FTT **63**, *8*, 1098 (2021). (in Russian). http://dx.doi.org/10.21883/FTT.2021.08.51160.077
[14] E.V. Dvoretskaya, V.L. Sidorov, O.V. Koplak, D.V. Korolev, V.P. Piskorsky, R.A. Valeev, R.B. Morgunov. FTT **64**, *8*, 984 (2022). (in Russian). http://dx.doi.org/10.21883/FTT.2022.08.52694.373
[15] S.F. Cheng, R. Segnan, J.R. Cullen, A.E. Clark, M.Q. Huang. J. Appl. Phys. **73**, *10*, 5733 (1993). https://doi.org/10.1063/1.353607
[16] E.N. Kablov, O.G. Ospennikova, V.P. Piskorsky, D.V. Korolev, E.I. Kunitsyna, A.I. Dmitriev, R.B. Morgunov. Fizika nizkikh temperatur, **42**,*1*, 60 (2016). (in Russian).
[17] E.I. Kunitsyna, V.P. Piskorsky, D.V. Korolev, R.A. Valeev, V.V. Kucheryaev, R.B. Morgunov. FTT **60**, *12*, 2384 (2018). (in Russian). http://dx.doi.org/10.21883/FTT.2018.12.46728.128
[18] J.B. Thoelke. Magnetization and magnetostriction in highly magnetostrictive materials. United States (1993). https://doi.org/10.2172/10190712
[19] Y.V. Yang, Y.Y. Huang, Y.M. Jin. Appl. Phys. Lett. **98**, *1*, 012503 (2011). https://doi.org/10.1063/1.3533910

*Translated by Ego Translating*